JOURNAL OF CATALYSIS 64, 381–396 (1980)

# Examination of Carbon-Supported Catalysts by Electron Microscopy

G. R. MILLWARD

*Department of Physical Chemistry, University of Cambridge, Lensfield Road, Cambridge CB2 1EP, England*

Received July 17, 1979; revised February 8, 1980

The routine application of bright-field high-resolution electron microscopy to the characterization of metal catalysts supported on graphitized carbon is discussed in terms of optimization of the imaging conditions. By suitable choice of objective aperture, and defocus, phase-contrast lattice-imaging of the graphitic support may be maintained while at the same time retaining most of the dark scattering contrast associated with the metal particles. Specific examples are given with a lower limit to particle detectability being, in general, about 1.5–2.0 nm.

## INTRODUCTION

Electron microscopy provides a direct means of obtaining information about the state of aggregation of supported metal catalysts. It yields supplementary evidence to that obtained by essentially averaging methods as, for instance, X-ray scattering, EXAFS or chemisorption, and in particular can tell us something about the homogeneity, or otherwise, of the catalyst system. Several groups of workers have reported using electron microscopy to study a variety of supported catalysts (*1–12*). In this paper we shall consider methods adopted for *routine* examination of platinum group metals attached to carbon supports using conventional bright-field high-resolution electron microscopy.

## METHODS

These studies were carried out using a Philips EM300 electron microscope fitted with the high-resolution stage (spherical aberration coefficient, $C_s$ = 1.6 mm). Standard filaments were used and the Wehnelt cap aperture was 0.5 mm. Condenser apertures were: first condenser—300 $\mu$m, second condenser—200 $\mu$m. Low gun emissions were employed (positions 1 or 2), in order to minimize Boersch effect spreading of energies in the electron source, and an accelerating potential of 100 kV was used. The choice of objective aperture can be crucial in all high-resolution studies; this factor will be discussed in the results section of this paper.

Specimens were crushed by agate mortar and pestle and dispersed into suspension by shaking in ethanol. A drop of the suspension was placed on a "holey-carbon" electron microscope specimen support (*13*) and allowed to dry. Micrographs were recorded only of regions of the specimen coinciding with a hole in the supporting film so that the latter does not contribute to the image.

## RESULTS

Our interest in the electron microscopy of supported catalysts arose from electron micrographs which ostensibly demonstrated the presence of dark Pt particles on a graphitized carbon black support (Fig. 1). The presence of large dense particles of Pt was undoubtedly revealed in these micrographs; but what was less clear was the provenance of the much smaller, but numerous, dark spots distributed randomly on the carbon support. High-resolution studies soon demonstrated that the majority of the small dots were merely strongly scattering crystalline regions of graphite (Fig. 2). Careful control of imaging conditions must, therefore, be maintained for successful differentiation between metal catalyst and the supportive medium (*14*), and we feel that an important criterion, in the present instance, is that the graphitic (0002) lattice



0021-9517/80/080381-16$02.00/0

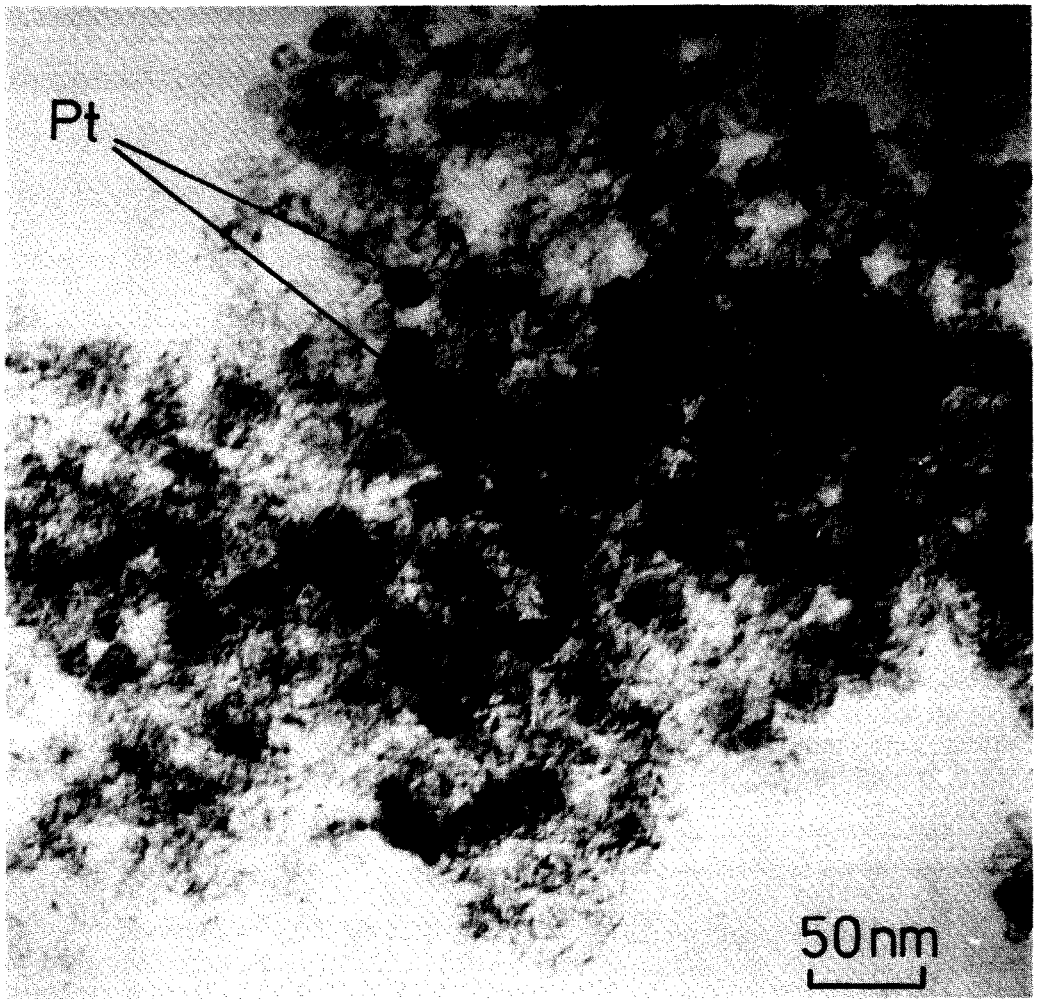


FIG. 1. Low-resolution image of Pt on graphitized channel black.

structure of the carbon support should be resolved.

*Phase-contrast lattice-imaging* of molecular layers requires that the diffracted electron beams, corresponding to the lattice of interest, be transmitted by the optical system with appropriate phase changes so that interference with the primary beam in the image plane yields fringes equivalent to the object lattice (shown diagrammatically in Fig. 3a). The phase-modification by the electron optical system is largely governed by the spherical aberration ($C_s$) and defect of focus (DF) of the objective lens (*15*), and can best be described in terms of transfer theory (*16–19*). In this theory the transfer of information from object plane to image plane is considered in terms of a phase transfer function operating in the diffraction plane of the objective lens. When the specimen is sufficiently thin in a direction parallel to the optic axis of the microscope (*20*), the transfer function assumes a relatively simple role and acts as a filter function transmitting information faithfully only when its value is +1. For any particular value of $C_s$ the transfer function can be optimized for *structural imaging* (i.e., as wide a range of spatial frequencies, and hence lattice spacings, as possible should


FIG. 2. High-resolution image of Pt on graphitized channel black.

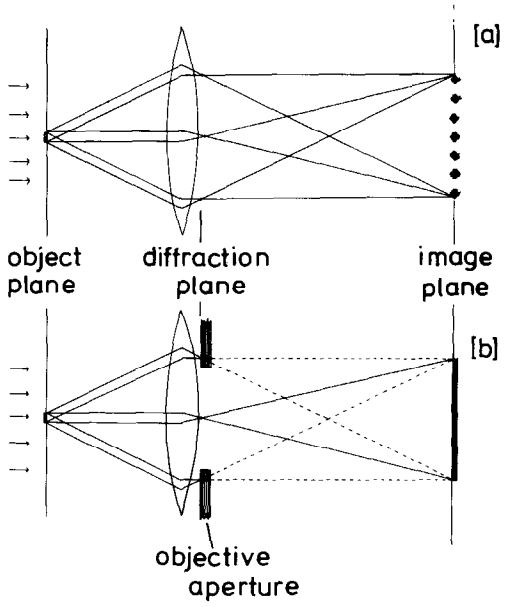


FIG. 3. Schematic optical diagram: (a) lattice imaging; (b) scattering contrast mechanism.

be encompassed by a continuous region of the function with an amplitude near to unity) by suitable choice of defocus.

In Fig. 4 we illustrate optimized transfer functions for three sets of aberration conditions. The functions shown are simple phase-contrast derivatives from which the effects of beam divergence, chromatic aberration, and electrical instabilities have been excluded. If such coherence factors are taken into consideration the amplitude of the function diminishes with increasing spatial frequency in a manner that can be defined by a "damping" envelope function (*16, 19, 21, 22*), which effectively designates the resolution limit of the microscope. However, in the case of the Philips EM300, and similar subsequent models, such factors are unlikely to affect, seriously, lattice image contrast corresponding to spatial frequencies less than 3.0 $nm^{-1}$ (*19*) provided that the spread of energies on the electron source is not made too large by the use of excessive gun brightness. For the present purposes where the highest resolution required is the (0002) graphite lattice fringes (already demonstrated to be imaged with adequate contrast—see Fig. 2), it is considered unnecessary to include such coherence factors in the transfer functions illustrated.

Figure 4A, the optimized phase contrast transfer function appropriate to a Philips EM300, is typical for high-resolution instruments of that generation. It is to be noted that exact structural lattice-imaging of graphite carbons is not entirely appropriate for this instrument since the transfer function results in severe attenuation at the special frequency pertaining to the basic 0.336-nm graphite interlayer periodicity (*19, 20, 23, 24*). The transfer function illustration in Fig. 4C ($C_s$ = 1.1 mm, DF = 70 nm under focus, 120 keV electrons) can be matched or bettered by most of the high-resolution microscopes now offered by the manufacturers and is much better adapted to structural imaging of graphitic materials (*19, 24*). Notwithstanding the promise of such recent improvements in instrumental performance, the limitations of the EM300, as suggested above, are not as intolerable as they might at first seem. For by varying the defocus of the objective lens in a controlled manner it is possible to obtain image-fringes that can be used to characterize graphitic structure (*19, 24–27*) although

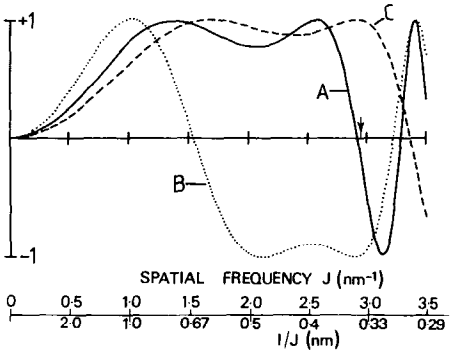


FIG. 4. Phase contrast transfer functions. (A) —— $C_s$ = 1.6 mm, DF = 92.5 nm underfocus; (B) · · · · · $C_s$ = 1.6 mm, DF = 140.0 nm underfocus, 100 keV electrons; (C) ----- $C_s$ = 1.1 mm, DF = 70 nm underfocus, 120 keV electrons. The spatial frequency corresponding to the 0.336 nm graphite lattice periodicity is indicated by the arrow.

there may not necessarily be a direct relationship between fringe and graphite layer (*19, 20, 24, 26, 28*). As an example (one of many possible) an underfocus value of 140 nm yields a transfer function (Fig. 4B) with an amplitude of $-1$ at the spatial frequency corresponding to the appropriate graphite periodicity. The fringes related to the graphite layers will appear with strong but negative contrast (*19*), although additional spacious fringes may occur in imperfectly ordered graphite systems (*19, 24, 28*) because of the inflexiom in the transfer function near 0.15 $nm^{-1}$. In the present application *fringe-imaging*, rather than *structural imaging*, can be adequate for differentiating between a well-graphitized carbon support and the metal catalyst particles, providing that suitably thin areas of specimen are chosen, and that the particles are not too small. Since most specimens of the type considered here exhibit significant three-dimensional characteristics, it should be borne in mind that differing areas of the specimen will be imaged at differing effective focal levels for any particular nominal value of the objective defocus. Any one micrograph will, in general, contain regions where the imaging conditions are good, and regions where they are less appropriate.

A particularly important consideration in setting the imaging conditions for this type of investigation is the choice of objective aperture. The diameter of the hole is required to be large enough to transmit the (0002) diffracted electrons from the graphitic support to enable phase-contrast lattice-fringe imaging as discussed above. At the same time we wish the *scattering contrast* of metal particles of a particular thickness to be maximized by absorbing as many as possible of the electrons Bragg scattered by the particles. The required absorption is provided, and governed, by the aperture in the back-focal plane of the objective lens (see Fig. 3b). Particles which scatter a significant proportion of electrons which are subsequently intercepted outside the aperture, will be deficient in electrons in the corresponding position of the image plane, and therefore appear darker on the screen (and darker on the photographic print of the image recorded on film) than the surrounding regions, other things being equal.

As an example we can consider the graphitized carbon black supported platinum catalyst shown earlier. Figure 5 shows an electron diffraction pattern from a region of the specimen 200 nm in diameter.

The contributions from the graphitic carbon (rings) and several Pt particles (spots) can be readily distinguished. Clearly, the perimeter of the optimum aperture for this system will lie between the (0002) graphite ring and the inner (111) Pt diffraction spots (=0.227 nm), as indicated by the dotted line (a) (Fig. 5). As required (0002) graphitic lattice imaging is allowed and all elastically Bragg diffracted electrons from crystalline Pt are absorbed outside the aperture. The aperture size corresponding to this position in a Philips EM300, of focal length 1.6 mm, operating at an accelerating potential of 100 kV is about 45 $\mu$m. The effect of increasing the aperture size from 45 $\mu$m to 70 $\mu$m [position (b) in Fig. 5] can be seen in Fig. 6. In both cases illustrated the structure of the carbon support is virtually identical, but the contrast of particle A, relative to the background, is less when the aperture is 70 $\mu$m than when the aperture is 45 $\mu$m. Diffracted electrons which are allowed to pass through to the image plane when the aperture is 70 $\mu$m in diameter are absorbed when the smaller aperture is used; hence, the scattering contrast is greater in the latter instance. Particle B (Fig. 6) does not exhibit such a change in contrast with aperture size because its particular orientation yields only Bragg diffracted beams that are outside the diameter of both apertures. A 70-$\mu$m aperture excludes all diffracted beams equivalent to a spacing of 0.169 nm or smaller, i.e., all Pt crystal lattices other than (111) at 0.227 nm and (002) at 0.196 nm. The 45-$\mu$m optimally sized aperture will eliminate all diffracted beams corresponding to spacings less than 0.263 nm and therefore has wide

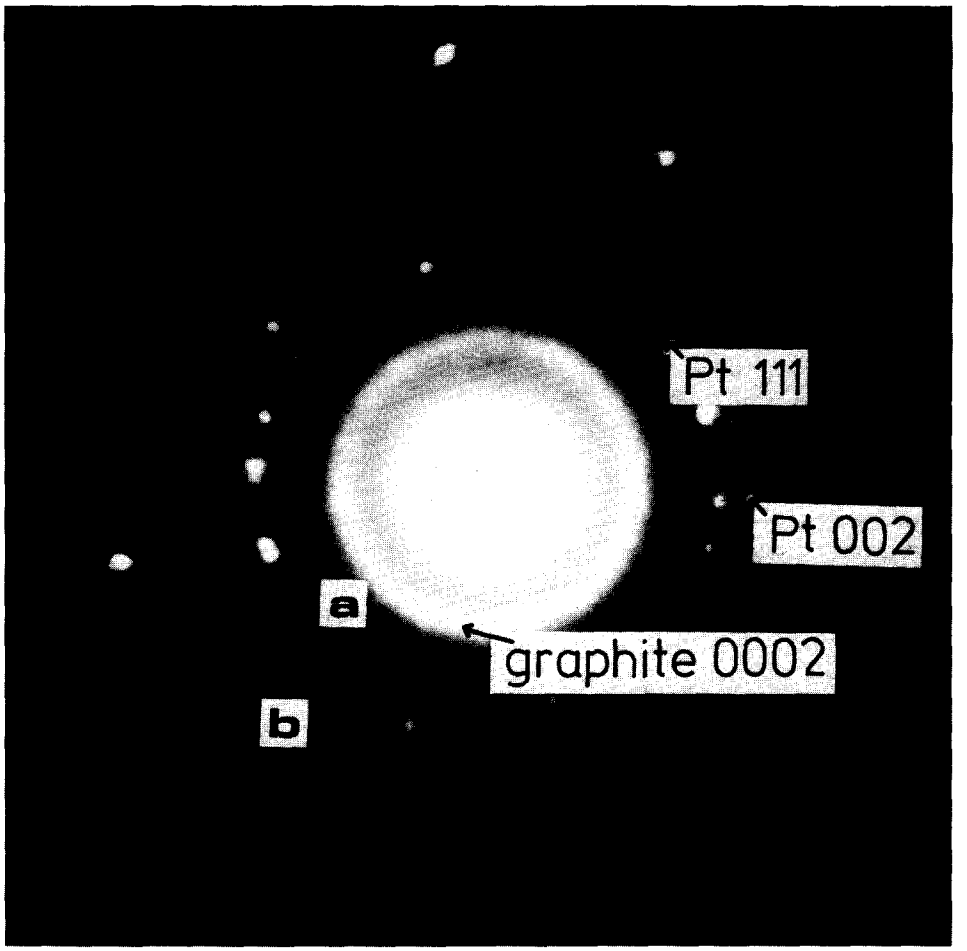


FIG. 5. Selected area (200 nm) diffraction pattern of group of Pt crystallites on graphitized channel black. (a) ≡ 45-$\mu$m aperture; (b) ≡ 70-$\mu$m aperture.

applicability for imaging many of the metals used in carbon-supported catalytic systems. In principle the aperture can be reduced in size to eliminate diffracted beams from larger spacings, provided the aperture does not interfere with (0002) graphitic diffracted electrons. In the case of the graphitized channel blacks illustrated in Figs. 1, 2, 5, and 6, this sets a lower limit of 37.5 $\mu$m (equivalent to a lattice periodicity of 0.315 nm) for the aperture diameter (some allowance has to be made for the broadening of the diffracted beam due to small crystal size). In practice apertures much less than 45 $\mu$m can cause difficulties in astigmatism correction, for the high resolution required, and should, if possible, be avoided.

Using the criteria outlined above, we have been able to characterize a variety of supported metal catalysts on a more or less routine basis. Figure 7 shows further examples of Pt on graphitized channel black; the particles were usually well dispersed (Fig. 7a), but sometimes appear in clumps (Fig. 7b). The particle size of the Pt depended on the method of preparation; for instance in one sample there was a fairly uniform distribution of particle sizes between 7 and 30 nm, while in another there was a variation between 1.5 and 12 nm but with a prepon-

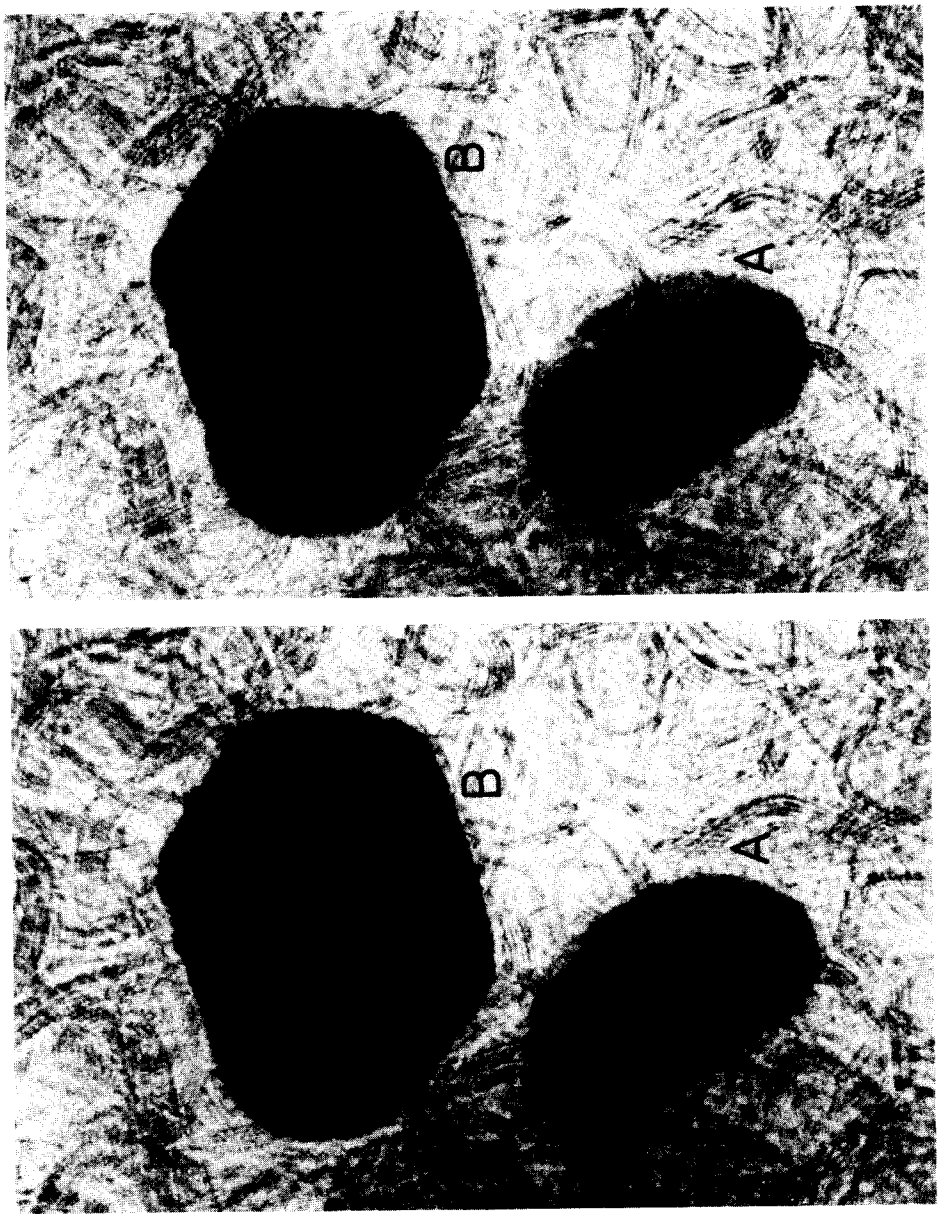


FIG. 6. Images of Pt particles on graphitized channel black: (a) with 45-$\mu$m objective aperture; (b) with 70-$\mu$m objective aperture.

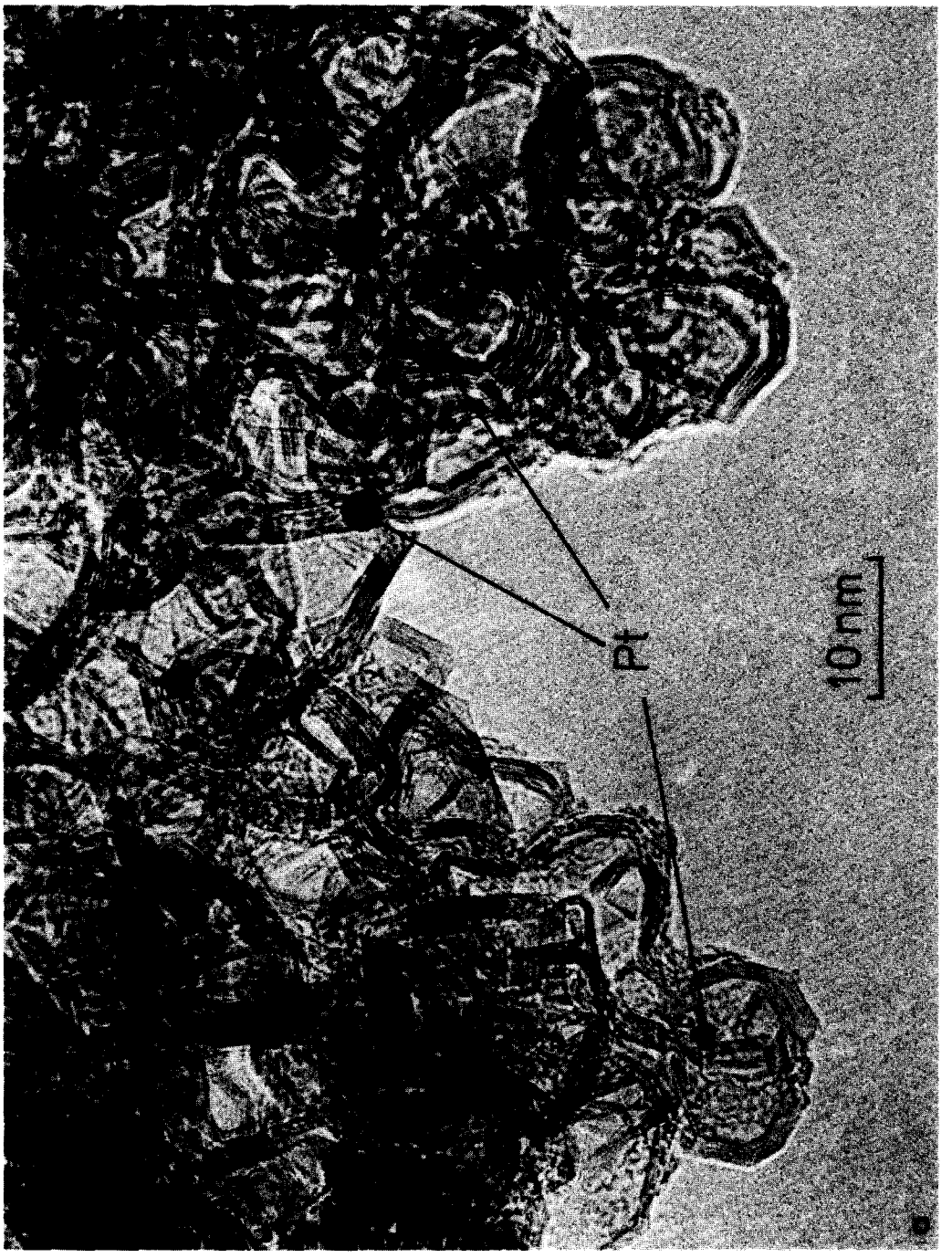
Pt
10 nm

FIG. 7. (a) and (b) High-resolution images of Pt on graphitized channel black.

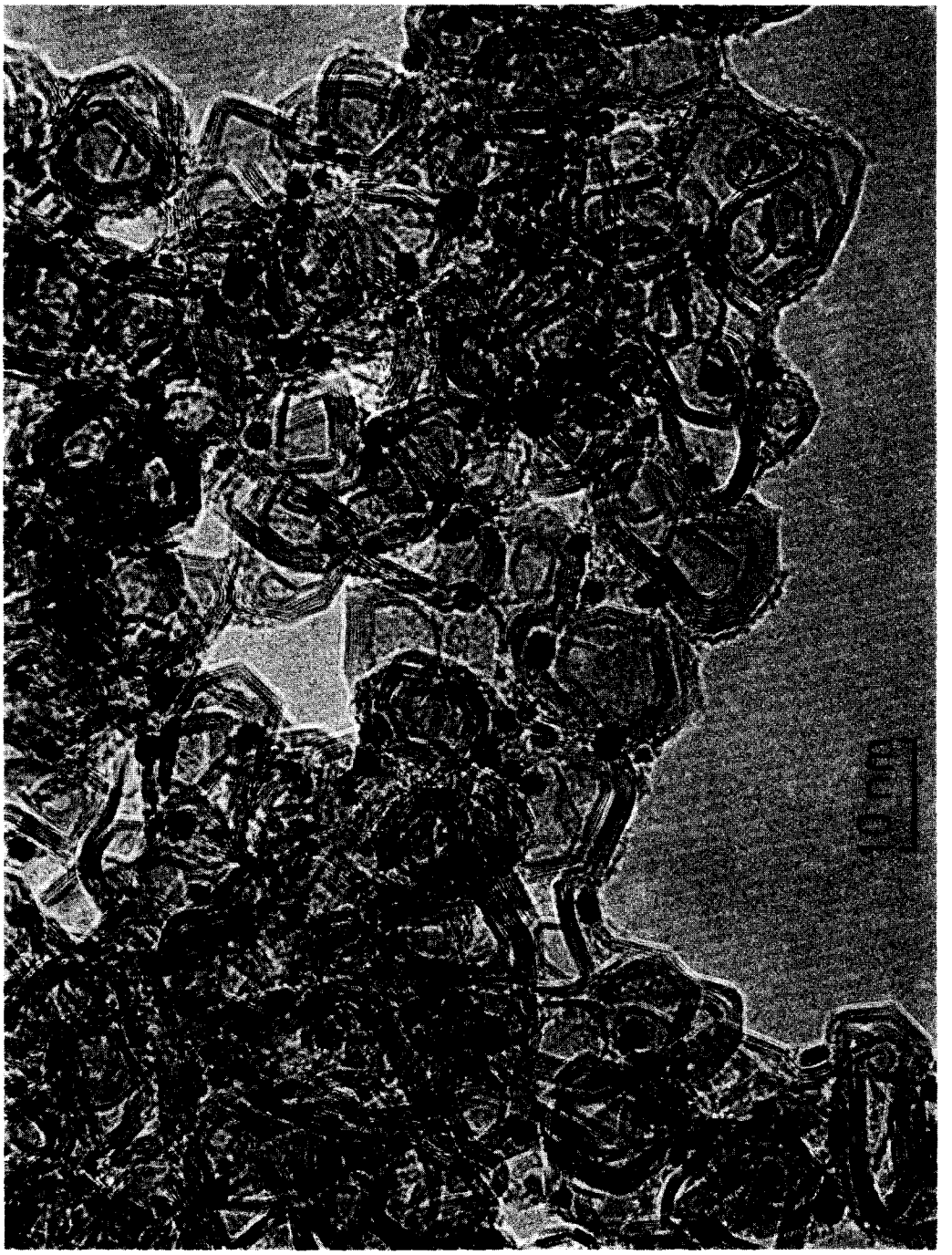


FIG. 8. High-resolution image of alkali-doped Pt-group catalyst on graphitized channel black.

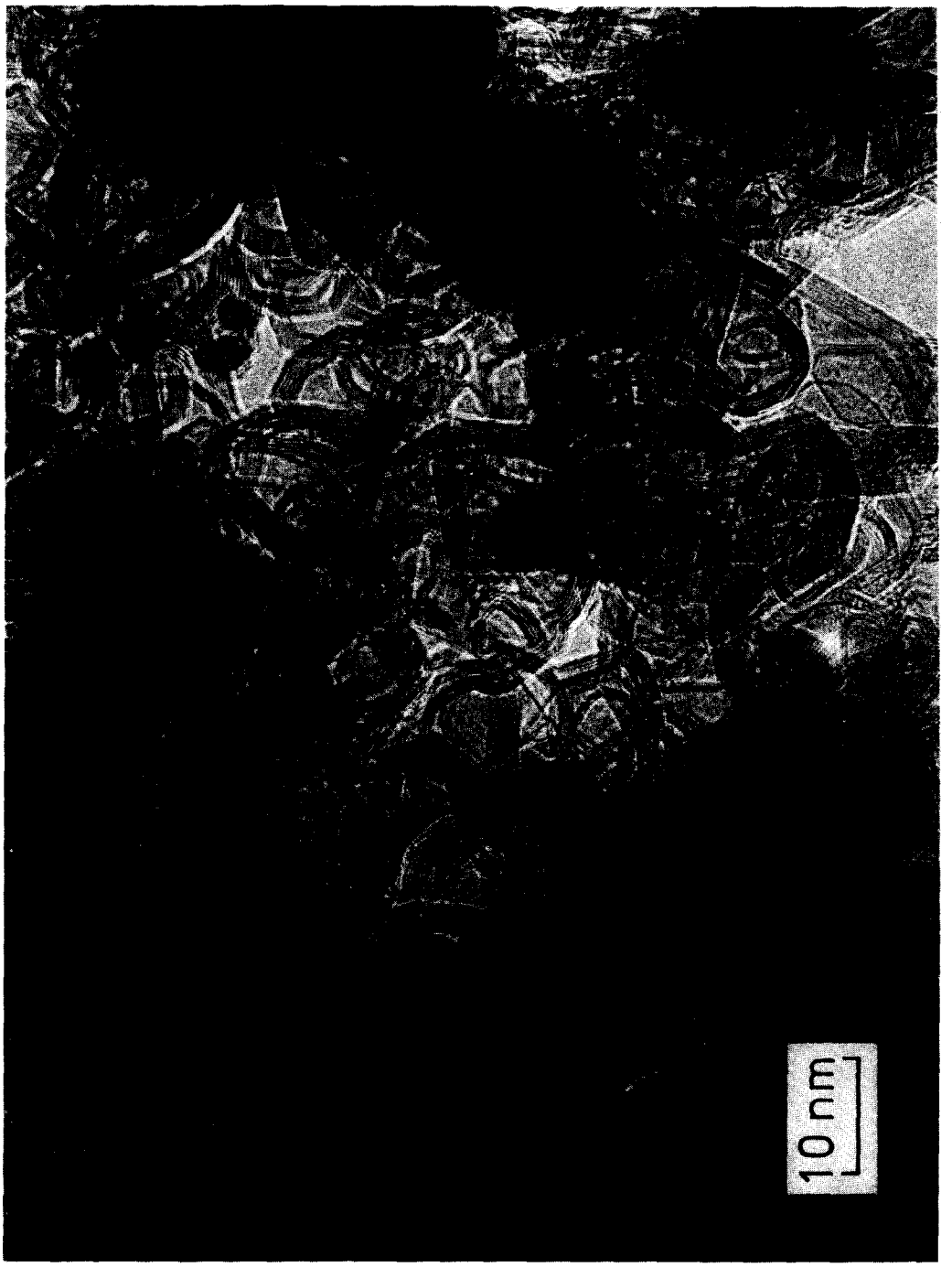


FIG. 9. High-resolution image of alkali-doped Pt-group catalyst on graphitized channel black; differently prepared sample to that corresponding to Fig. 8.

derance of particles between 2 and 4 nm in diameter.

Figures 8 and 9 illustrate examples of images of two types of alkali-doped platinum-group catalyst metals on graphitized channel black. In the former case the particles are quite evenly distributed over the support and range in size between 1.5 and 5 nm; however, in the sample relevant to Fig. 9 the particles possess a wider range of diameters (3–15 nm), are relatively unevenly distributed, and often their shape (for reasons which we do not as yet fully understand) is not well defined.

Figure 10 is a typical micrograph of a Pt catalyst prepared on a partially oxidized graphitized carbon paper. The Pt is fairly evenly dispersed and particles have been observed of diameter from 0.7 up to 5 nm. In a Pt/Ru mixed catalyst prepared on carbon paper after $CO_2$ treatment the metal was distributed unevenly in large aggregates of small (1.5–3 nm) particles (Fig. 11).

## DISCUSSION

This paper has been restricted to a consideration of the application of straightforward high-resolution electron microscopy to the study of graphitic-carbon-supported metal catalysts. Suitable equipment is now available in many laboratories for such study, which is less time consuming and more amenable to routine investigations than the appreciably more expensive, but inherently more precise, ultrahigh vacuum scanning transmission electron microscope systems.

Metal particles of size greater than about 2 nm, when supported on graphitized carbon, can be recognized as such with reasonable confidence provided that the support is thin (e.g., Fig. 7). However, where the supporting material is scattering particularly strongly because it is thicker, or where graphitic crystalline regions overlap appropriately, metal particles may be obscured or assignment made uncertain. Lattice resolution of the supporting structures greatly reduces the danger of strongly contrasted graphitic regions being mistaken for metal particles. In our experience it is difficult to detect metal particles smaller than 1.5–2 nm on graphitized carbon supports. Only in favorable circumstances, for example in Fig. 10 where in some regions the catalyst support is thin and oriented so that (0002) graphite lattice diffraction is absent, can smaller particles (0.5–1 nm) be distinguished. The relative insensitivity of the technique for detecting the smaller particle is, at present, one of its limitations, and it has to be recognized that particle size distribution measurements will involve attenuation of histograms at the smaller values of diameter.

By using instruments with better electron optical aberration properties, so that structural imaging of the graphitic support can be obtained rather than fringe-imaging, the ability to differentiate between metal particle and support should be improved, with a possible bonus of information about aspects of the environment of the catalyst in relation to the supporting carbon assembly also becoming available. Additionally, the detectability of particles can be enhanced, in certain circumstances, by utilizing specialized electron optical equipment such as hollow-cone dark-field electron microscopy (*29*) or the various modes of imaging available on scanning transmission instruments (*30*).

Optimization of the imaging conditions has been considered, in this paper, in terms of phase contrast lattice-fringe imaging of the carbon support (controlled by objective defocus), coupled with maximizing the scattering contrast of the metal particles by suitable choice of objective aperture. Such control is readily applied by the electron microscopist. Nevertheless it should be remembered, particularly when considering a detailed interpretation of image contrast, that sources of contrast other than those considered here almost certainly operate concurrently (*29–32*). Reference to Fig. 8 shows that the contrast of the metal particles is not directly related to their lateral

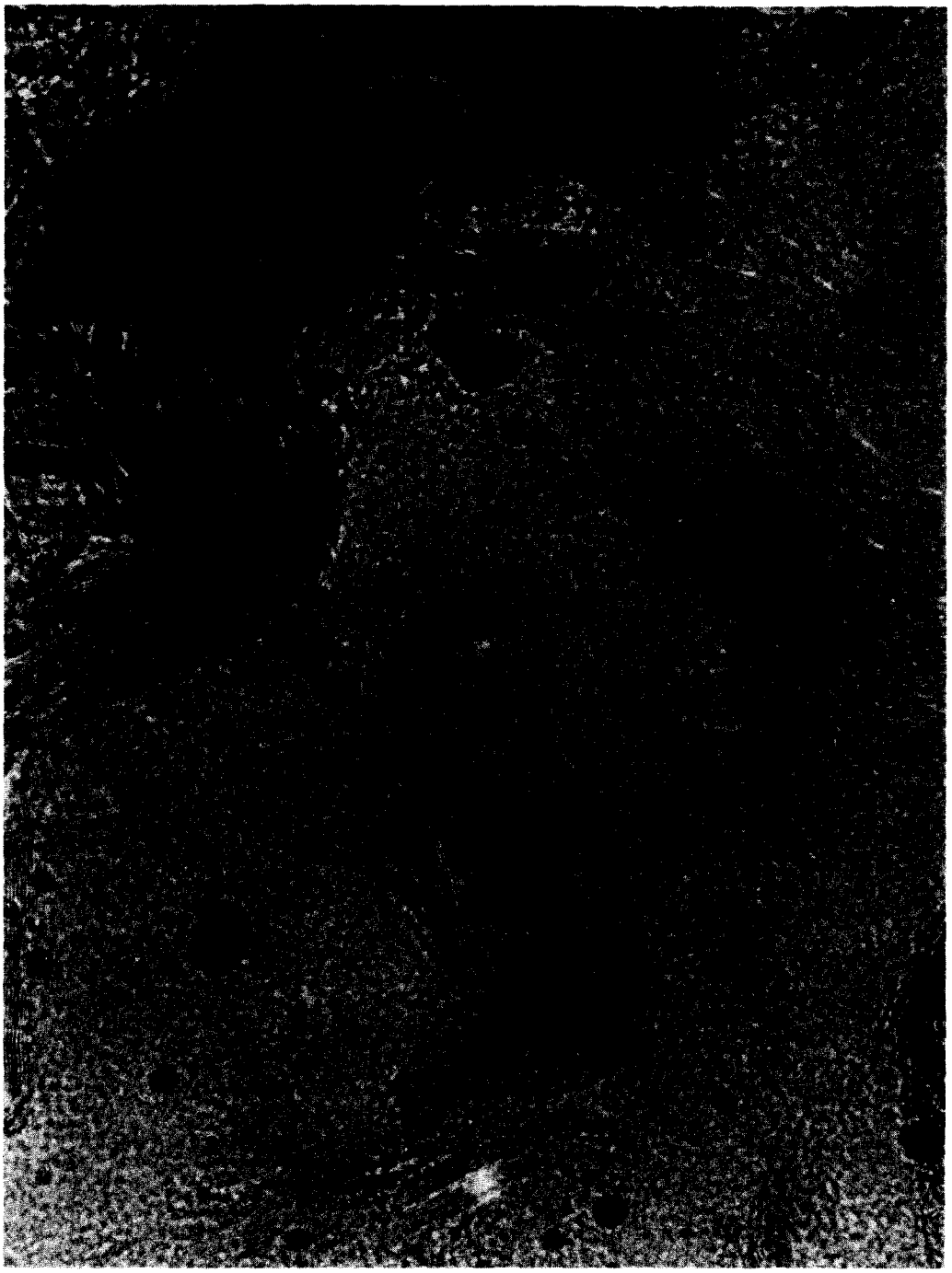

FIG. 10. High-resolution image of Pt catalyst on graphitized carbon paper.


FIG. 11. High-resolution image of Pt/Ru mixed catalyst on graphitized carbon paper.

diameter, i.e., the largest particles are not always the darkest. It is tempting to suggest, on the basis of our relatively simple treatment, that the more transparent particles are very thin and possess a flat raft-like geometry (*8*). However, as Flynn and Wanke (*31*) have pointed out, the scattering contrast of such particles is strongly dependent upon the crystallographic orientation with respect to the electron beams. Such contrast is also dependent upon specimen thickness, but because multiple scattering can yield an increase or a decrease in the intensity of particular scattered beams as the specimen thickness increases (*18–20*), the interpretation of contrast directly in terms of specimen thickness is not straightforward. Furthermore, phase shifts in the electron waves passing through the particle (and objective aperture) can, in combination with the electron optical transfer properties of the microscope, yield an additional contrast component which varies with objective defocus (*29–32*). For these reasons it is unwise, generally, to correlate the thickness of crystalline particles directly with dark intensity in the electron micrograph.

Finally, it has to be remembered that a typical electron microscope study of a catalyst preparation is, in effect, a postmortem examination. The catalyst is not in its normal operating environment and may have been modified during preparation as a specimen suitable for insertion into an electron microscope. In the present study the observed differences between specimens were consistent and therefore reflect genuine differences in the original catalysts. Notwithstanding this, there is obviously considerable scope for determining the effects of specimen preparation on, for instance, the dispersion of metal particles throughout the support.

## ACKNOWLEDGMENTS

The author acknowledges the help and encouragement of Professor J. M. Thomas, and the support and facilities provided by the National Coal Board and the Science Research Council. I am indebted to Mr. S. R. Tennison of BP Research Centre, Sunbury, and Dr. J. O. Williams of the Edward Davies Chemical Laboratory, Aberystwyth, for specimens and discussions.

## REFERENCES

1. Adams, C. R., Penesi, H. A., Curtis, R. M., and Meisenheimer, R. G., *J. Catal.* **1,** 336 (1962).
2. Cormack, D., and Moss, R. L., *J. Catal.* **13,** 1 (1969).
3. Avery, N. R., and Sanders, J. V., *J. Catal.* **18,** 129 (1970).
4. Pope, D., Smith, W. L., Eastlake, M. J., and Moss, R. L., *J. Catal.* **22,** 72 (1971).
5. Renouprez, A., Hoang-Van, C., and Compagnon, P. A., *J. Catal.* **34,** 411 (1974).
6. Basset, J. M., Dalmai-Imelik, G., Primet, M., and Mulu, R., *J. Catal.* **37,** 22 (1975).
7. Anderson, J. R., "The Structure of Metallic Catalysts. Academic Press, London, 1975.
8. Prestridge, E. B., Via, G. H., and Sinfelt, J. H., *J. Catal.* **50,** 115 (1977).
9. Chu, Y. F., and Ruckenstein, E., *Surface Sci.* **67,** 517 (1977).
10. Hamilton, J. F., and Logel, P. C., *J. Catal.* **29,** 253 (1973).
11. Hamilton, J. F., and Logel, P. C., *Thin Solid Films* **16,** 49 (1973).
12. Hamilton, J. F., and Logel, P. C. *Thin Solid Films* **23,** 89 (1973).
13. Fukami, A., and Adachi, K., *J. Electromicr.* **14,** 112 (1965).
14. Prestridge, E. B., and Yates, D. J. C., *Nature (London)* **234,** 345 (1971).
15. Scherzer, O., *J. Appl. Phys.* **20,** 20 (1949).
16. Hanzen, K. J., *Adv. Opt. Electron Microsc.* **4,** 1 (1971).
17. Hoppe, W., *Acta Crystallogr.* **A26,** 414 (1970).
18. Cowley, J. M., "Diffraction Physics." North Holland, Amsterdam, 1975.
19. Milward, G. R., and Jefferson, D. A., *Chem. Phys. Carbon* **14,** 1 (1979).
20. Jefferson, D. A., Millward, G. R., and Thomas, J. M., *Acta Crystallogr.* **A32,** 823 (1976).
21. Hanzen, K. J., and Trepte, L., *Optik* **32,** 519 (1971).
22. Frank, J., *Optik* **44,** 379 (1976).
23. Millward, G. R., and Thomas, J. M., *Proc. 4th Int. Conf. Ind. Carbon and Graphite,* London, 1974, Soc. Chem. Ind., London (1976), p. 492.
24. Millward, G. R., and Thomas, J. M., *Carbon* **17,** 1 (1979).
25. Heidenreich, R. D., Hess, W. M., and Ban, L. L., *J. Appl. Cryst.* **1,** 1 (1968).
26. Millward, G. R., Jefferson, D. A., and Thomas, J. M., *J. Microsc.* **113,** 1 (1978).

27. Ban, L. L., *Surface Defect Prop. Solids* **1**, 54 (1972).
28. Crawford, D. A., and Marsh, H., *J. Microsc.* **109**, 145 (1977).
29. Freeman, L. A., Howie, A., and Treacy, M. M. J., *J. Microsc.* **111**, 165 (1977).
30. Treacy, M. M. J., Howie, A., and Wilson, C. J., *Phil. Mag.* **A38**, 569 (1978).
31. Flynn, P. C., and Wanke, S. E., *J.Catal.* **33**, 233 (1974).
32. Hall, C. R., and Hines, R. L., *Phil. Mag.* **21**, 1175 (1970).